Supersaturation in the Wake of a Precipitating Hydrometeor and its Impact on Aerosol Activation

Geophysical Research Letters

RESEARCH LETTER
10.1029/2020GL091179

Key Points:
- This study shows how hydrometeor wake-induced supersaturation in clouds activates aerosols as cloud condensation nuclei
- The parameter space for wake-induced supersaturation behind precipitating spherical hydrometeors is detailed
- It is described how lucky aerosols are activated in such supersaturated wake of the precipitating hydrometeors

Supporting Information:
- Supporting Information S1

Correspondence to:
Y. Wang and G. Bagheri,
yong.wang@ds.mpg.de;
gholamhossein.bagheri@ds.mpg.de

Citation:
Bhowmick, T., Wang, Y., Iovieno, M., Bagheri, G., & Bodenschatz, E. (2020). Supersaturation in the wake of a precipitating hydrometeor and its impact on aerosol activation. *Geophysical Research Letters*, *47*, e2020GL091179. https://doi.org/10.1029/2020GL091179

Received 22 JUL 2020
Accepted 6 NOV 2020
Accepted article online 16 NOV 2020

Supersaturation in the Wake of a Precipitating Hydrometeor and Its Impact on Aerosol Activation

Taraprasad Bhowmick[1,2], Yong Wang[2], Michele Iovieno[3], Gholamhossein Bagheri[2], and Eberhard Bodenschatz[2,4,5]

[1]Department of Applied Science and Technology, Politecnico di Torino, Torino, Italy, [2]Laboratory for Fluid Physics, Pattern Formation and Biocomplexity, Max Planck Institute for Dynamics and Self-Organization, Göttingen, Germany, [3]Department of Mechanical and Aerospace Engineering, Politecnico di Torino, Torino, Italy, [4]Institute for Dynamics of Complex Systems, University of Göttingen, Göttingen, Germany, [5]Laboratory of Atomic and Solid State Physics, Cornell University, Ithaca, NY, USA

Abstract The activation of aerosols impacts the life cycle of a cloud. A detailed understanding is necessary for reliable climate prediction. Recent laboratory experiments demonstrate that aerosols can be activated in the wake of precipitating hydrometeors. However, many quantitative aspects of this wake-induced activation of aerosols remain unclear. Here, we report a detailed numerical investigation of the activation potential of wake-induced supersaturation. By Lagrangian tracking of aerosols, we show that a significant fraction of aerosols are activated in the supersaturated wake. These "lucky aerosols" are entrained in the wake's vortices and reside in the supersaturated environment sufficiently long to be activated. Our analyses show that this wake-induced activation of aerosols can contribute to the life cycle of the clouds.

Plain Language Summary We numerically investigate how new water droplets or ice particles are formed within a cloud. Out of several proposed physical processes for droplet generation, recent experimental studies have shown that a large droplet can nucleate aerosols in the wake behind it when falling under gravity. We present a detailed analysis of various physical factors that lead to an excess of water vapor behind the hydrometeors (e.g., droplets, sleet, or hail) and investigate the effectiveness of this process on activation of aerosols to create new cloud particles.

1. Introduction

The dynamics of atmospheric clouds remains a major source of uncertainty in weather and climate models (Stevens & Bony, 2013) due to the interplay of many physical processes over a wide range of scales (Bodenschatz et al., 2010). Especially, the activation of aerosols and species therein controls the lifetime of a cloud (Kreidenweis et al., 2019) in which fractions of cloud condensation nuclei (CCN) and ice nucleating particles (INPs) develop into new hydrometeors (Baker, 1997). Physical processes contributing to the production of secondary ice particles (Field et al., 2017) within a mature cloud cannot explain the observed discrepancies between the measured activation and the observed hydrometeor population, which is several orders of magnitude higher than expected (Huang et al., 2017; Pruppacher & Klett, 2010). One possible explanation of this riddle might be the wake-induced supersaturation (Chouippe et al., 2019; Fukuta & Lee, 1986; Gagin, 1972) and activation of aerosols behind large precipitating hydrometeors, that is, heterogeneous wake-induced nucleation (Prabhakaran et al., 2020). The experimental investigation by Prabhakaran et al. (2017) of falling drops (diameter of $\mathcal{O}(1)$ mm) in near critical point conditions of pressurized sulfur hexafluoride showed the evidences of homogeneous nucleation in the wake.

Prabhakaran et al. (2020) conducted a follow-up experiment on heterogeneous nucleation using sodium chloride and silver iodide aerosols under atmosphere-like conditions. Warm droplets with a diameter of ~2 mm were able to induce the activation of aerosols as water droplets and ice crystals in their wake when precipitating through a subsaturated colder environment. Earlier, a numerical analysis of supersaturation in the wake of a warmer hydrometeor moving through various colder environments was performed by

Chouippe et al. (2019). Their work confirms the existence of a supersaturated region in the wake of a hydrometeor that settles through a colder saturated environment. The maximum supersaturation observed in the wake was higher when the temperature difference between the hydrometeor and the ambient was larger. In a more recent study, Krayer et al. (2020) extended their earlier work Chouippe et al. (2019) and explicitly estimated the influence of wake supersaturation on the ice enhancement factor using a model based on a power law dependence of the local supersaturation (Baker, 1991; Huffman, 1973) and concluded that the local ice nucleation enhancement alone cannot produce a sufficient number of activated ice nuclei to solve the observed number discrepancy of measured ice particle concentration in clouds.

Although the development of supersaturation was studied numerically, the direct calculation of droplet or ice nucleation on cloud aerosols remained quite difficult due to the large number of influencing parameters which include size distribution (Dusek et al., 2006), number concentration (Baker, 1997), chemical composition (DeMott et al., 2018), porosity, or solubility (Kanji et al., 2017) of the aerosols, along with the presence of various bio or ion species inside clouds (Curtius, 2009). The complexity in the nucleation of ice on aerosols is further complicated in mixed-phase clouds containing both water and ice phase hydrometeors. Ice nucleation through deposition and condensation freezing can occur on an aerosol during supersaturation in the ice phase at subzero temperatures (Meyers et al., 1992). Ice production by immersion freezing on a CCN or by contact freezing on a supercooled water drop can also be observed (Dye & Hobbs, 1968; Kanji et al., 2017). The activation of aerosols as a CCN or an INP happens through different physical and chemical processes, which are active at different thermodynamic, cloud, and aerosol conditions. For example, Petters and Wright (2015) evidenced that a negligible concentration of INP exists at a cloud temperature higher than -5°C, while the concentration of INP at cloud temperatures between -5 °C and -15°C can vary up to 5 orders of magnitude. This variability in the number concentration of INP decreases as the temperature of the clouds reduces (Hader et al., 2014; Petters & Wright, 2015). The review by Hoose and Möhler (2012) presents a general overview of the various INP production processes, such as immersion freezing, deposition nucleation, contact nucleation, evidencing their strong dependence on the ambient temperature, supersaturation condition, and the aerosol species.

The above-mentioned studies elucidated some aspects of wake supersaturation and aerosol activation. In this letter, we present a comprehensive numerical study covering the parameter space relevant for atmospheric situations. We quantify the influences of ambient humidity and ambient/hydrometeor temperatures on the supersaturation within the wake for different sizes and phases of spherical hydrometeors. Next, with Lagrangian tracking of aerosols as passive tracers around such sedimenting hydrometeors, we quantify the residence time and supersaturation experienced by individual aerosols as a function of the governing parameters. Finally, we discuss how these results can help to quantify the likelihood and significance of heterogeneous wake-induced nucleation of aerosols in the atmospheric clouds.

2. Model and Methods

We numerically simulate the flow around a spherical hydrometeor with diameter d_p and temperature T_p falling in cloudy air (ambient: temperature T_∞, relative humidity RH_∞, density ρ_a, and pressure p_∞) with constant velocity U_p. While in general the shape of the hydrometeor will not be spherical, we expect this to be a good approximation. In the simulation all parameters are assumed to be constant, as the hydrometeor's and environment's properties vary slowly compared to that of the momentary flow (for more details see sections S2 and S3 in the supporting information).

In dimensionless form the incompressible Navier-Stokes (NS) equations and the one-way coupled advection-diffusion (AD) equations for temperature and water vapor density are

$$\nabla \cdot \mathbf{u} = 0, \tag{1}$$

$$\frac{\partial \mathbf{u}}{\partial t} + \mathbf{u} \cdot \nabla \mathbf{u} = -\nabla p + \frac{1}{Re} \nabla^2 \mathbf{u}, \tag{2}$$

$$\frac{\partial T}{\partial t} + \mathbf{u} \cdot \nabla T = \frac{1}{RePr} \nabla^2 T, \tag{3}$$

$$\frac{\partial \rho_v}{\partial t} + \mathbf{u} \cdot \nabla \rho_v = \frac{1}{Re\,Sc} \nabla^2 \rho_v, \tag{4}$$

where p is the dimensionless pressure $(p - p_\infty)/\rho_a U_p^2$, $Re = U_p d_p/\nu$ is the Reynolds number (with ν being the kinematic viscosity of air), $Pr = \nu/\kappa$ is the Prandtl number (with κ being the thermal diffusivity of air), and $Sc = \nu/\kappa_v$ is Schmidt number (with κ_v being the water vapor diffusivity). Following Kotouč et al. (2009) and Krayer et al. (2020), as a first approximation, we neglect evaporation feedback on the momentum and particle temperature in the simulations (see section S4 in the supporting information).

We solve the model equations with the lattice Boltzmann method (LBM) (Guo et al., 2002; Krüger et al., 2017; Qian et al., 1992; Silva & Semiao, 2012; Succi, 2001; Tian et al., 2018) within the open-source LBM library Palabos (Latt et al., 2020). The simulation domain, with reference frame in the center of the hydrometeor, extends $[-5, 20]d_p \times [-3.5, 3.5]d_p \times [-3.5, 3.5]d_p$ with a uniform Cartesian mesh of grid size $d_p/32$. The surface of the hydrometeor is no-slip at zero velocity and with a constant temperature T_p and water vapor density $\rho_{v,p} = \rho_{vs}(T_p)$, which is saturated at T_p according to Maxwell diffusion model. The transport of momentum and scalars in the steady wake of a sphere is discussed in Bhowmick et al. (2020) using the same numerical method.

3. Results

We analyze the flow at different Reynolds numbers in the steady axisymmetric wake ($0 \le Re \le 220$) and in the steady oblique wake ($225 \le Re \le 285$) (see Johnson & Patel, 1999; Tomboulides & Orszag, 2000), with $Pr = 0.71$ and $Sc = 0.61$ according to the values of the atmospheric standard conditions (Michaelides, 2006; Montgomery, 1947). In the case of a liquid hydrometeor of density 10^3 kg m^{-3}, these Re corresponds to hydrometeors with diameter between 3×10^{-4} m and 1.03×10^{-3} m falling with terminal velocities between 1.21 and 4.03 m s^{-1}. The ambient relative humidity RH_∞ is varied from nearly saturated ($RH_\infty \sim 100\%$) within the cloud (Siebert & Shaw, 2017) to a highly subsaturated condition in the open atmosphere (see also Prabhakaran et al., 2020). The supersaturation $S = RH - 1 = \rho_v/\rho_{vs}(T) - 1$ is computed with respect to the water phase when $T > 0°$C and with respect to the ice phase when $T \le 0°$C by using the following empirical Equations 5 and 6 for liquid and frozen hydrometeors, respectively (Huang, 2018).

$$\rho_{vs}(T)_{(T>0°\mathrm{C})} = \frac{1}{R_v(T + 273.15)} \frac{\exp(34.494 - 4924.99/(T + 237.1))}{(T + 105)^{1.57}}, \tag{5}$$

$$\rho_{vs}(T)_{(T\le 0°\mathrm{C})} = \frac{1}{R_v(T + 273.15)} \frac{\exp(43.494 - 6545.8/(T + 278))}{(T + 868)^2}. \tag{6}$$

We identify each simulations with a defined nomenclature, for example, "LC 0 15 90." Here the first letter indicates the hydrometeor phase (L liquid or I ice), the second letter indicates the sign of the temperature difference between the hydrometeor and the ambient (W warmer hydrometeor or C colder hydrometeor), and the three following numbers give the hydrometeor temperature T_p (in degrees Celsius), the modulus of $T_p - T_\infty$ referred as ΔT (in degrees Celsius) and the ambient relative humidity RH_∞ (in %). Thus, "LC 0 15 90" is a liquid hydrometeor colder than the ambient, with a surface temperature of 0°C in an ambient air with a temperature of 15°C and a relative humidity equal to 90%.

3.1. Supersaturation in the Wake

Figure 1a shows an example of a visualization of the supersaturation field at $Re = 275$ in an ambient relative humidity of 90% with respect to ice phase for a warm hydrometeor (IW 0 15 90). High supersaturation is clearly visible in the boundary layer of the droplet and in the near wake, as well as in the large region downstream of the hydrometeor. In this oblique regime, some streamlines pass through the wake's vortices, a feature consistent with the results of Johnson and Patel (1999) for the oblique wake vortex structures. The overall distribution of the supersaturated sample volume in the entire three-dimensional domain above a supersaturation threshold of $S_0 > 1 \times 10^{-4}$ is shown in Figure 1b. There the supersaturation spectrum $Sp(S)$, which gives the distribution of the supersaturated volume for various supersaturation magnitudes, is normalized by the hydrometeor volume and the supersaturated volume $V_S = \int_{S_0}^{S_{max}} Sp(S)\mathrm{d}S$ is an integral of $Sp(S)$. To avoid numerical round-off errors around the surface of the hydrometeor, where $S = 0$, the supersaturation threshold is defined as 1×10^{-4}, with S_{max} being the maximum supersaturation obtained in a

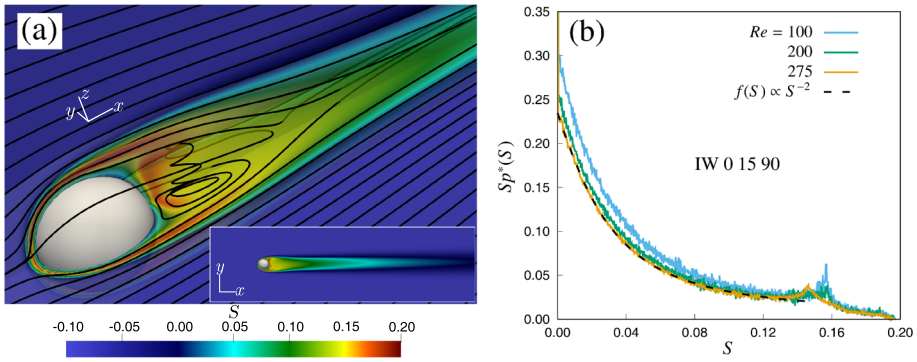

Figure 1. Spatial distribution of S. (a) Contours of S in two orthogonal central planes and complex streamlines for $Re = 275$. Only the region near the hydrometeor is plotted, while the entire two-dimensional domain along the orthogonal (x, y) plane is in the inset. (b) Normalized sample population spectrum $Sp^*(S) = Sp(S)/(\pi d_p^3/6)$ for various magnitudes of supersaturation ($S > 0$) over the entire three-dimensional domain for the case "IW 0 15 90" for the $Re =$ 100, 200, and 275. "IW 0 15 90" represents a (I) frozen but (W) warmer hydrometeor with (0) $T_p = 0°C$ in an ambient at $T_\infty = -15°C$, which gives (15) $\Delta T = 15°C$ and (90) $RH_\infty = 90\%$ with respect to the (I) ice phase.

simulation. The statistics of the bright-colored supersaturated region in Figure 1a shows the evolution $\propto S^{-2}$ in Figure 1b. This scaling in the distribution of the samples follows a Cauchy-Lorentz function, which is detailed in Bhowmick et al. (2020), and appears as a typical feature in the spatial distribution of the momentum and the transported scalars in the steady wake regime due to the balance between the advection and the diffusion. This trend of S^{-2} ceases around $S \geq 0.13$, which is the highest magnitude of S reached within the boundary layer and in the recirculating zone behind the hydrometeor in Figure 1a. $Sp(S)$ decreases slightly with increasing Reynolds number, which implies a reduction in the volume of the supersaturated region with respect to the hydrometeor volume, due to gradual thinning of the boundary layer and a correlated shrinking of the lateral extent of the wake. Although a volumetric change in V_S is observed with different Re, the magnitudes of S_{max} remain almost constant for a specific thermodynamic state, independent of Re.

The evolution of V_S as a function of Re and other thermodynamic parameters is shown in Figure 2a for exemplary cases presenting a temperature difference ΔT of 15°C and $RH_\infty = 95\%$. For full details on the evolution of V_S in a whole range of Re, ΔT, RH_∞, hydrometeor phase (I or L), and warmer (W) or cooler (C) setups, see section S5 in the supporting information. In general, a frozen hydrometeor (solid lines) produces a significantly larger supersaturated region than a liquid hydrometeor (dashed lines). This is partly due to the lower magnitude of the saturation vapor pressure in the ice phase compared to its magnitude in the liquid water phase at temperatures of <0°C (e.g., 13.7% lower at −15°C). The evolution of V_S, as shown in Figure 2a, with respect to the hydrometeor phase and its warmer or colder state also applies to all other ΔT and RH_∞, as detailed in the supporting information. Figure 2a also shows that warmer liquid droplets, as for example, "LW 15 15 95" in $T_\infty = 0°C$ produce almost 2.3–2.5 times larger V_S than ice hydrometeors like "IC -15 15 95." This is generally true also for other ΔT and RH_∞. This signifies that the warmer hydrometeors produce larger V_S than the colder ones for similar T_∞, ΔT, and RH_∞. This phenomenon can be further explained by analytically solving the normalized T and ρ_v equations (see section S6 in the supporting information) for $Re \sim 0$, where warmer liquid droplets like "LW 15 15 RH_∞" also produce larger V_S than the colder frozen hydrometeors as "IC -15 15 RH_∞" for various RH_∞ conditions. It is further observed that for warmer hydrometeors, a minimum of $\Delta T = 4 - 10°C$ is necessary to produce $V_S \sim \mathcal{O}(1) \times \pi d_p^3/6$, which are merely thin supersaturated boundary layers around the hydrometeor. For hydrometeors that are colder than the ambient, ΔT needs to be at least 6–12°C to produce a similar volume of V_S.

In all cases, the supersatured volume can be fitted by the following scaling function (goodness of fit 99.8%) for the whole range of the Reynolds number, despite the change in the wake structure around $Re = 220$.

$$V_S = C_0(1 + C_1 Re^\alpha) \tag{7}$$

The fitting coefficient C_0 represents an asymptotic value, which depends on the thermodynamic parameters of the ambient and the hydrometeors, that is, ΔT, RH_∞, (I) ice or (L) liquid, and (W) warm or (C) colder

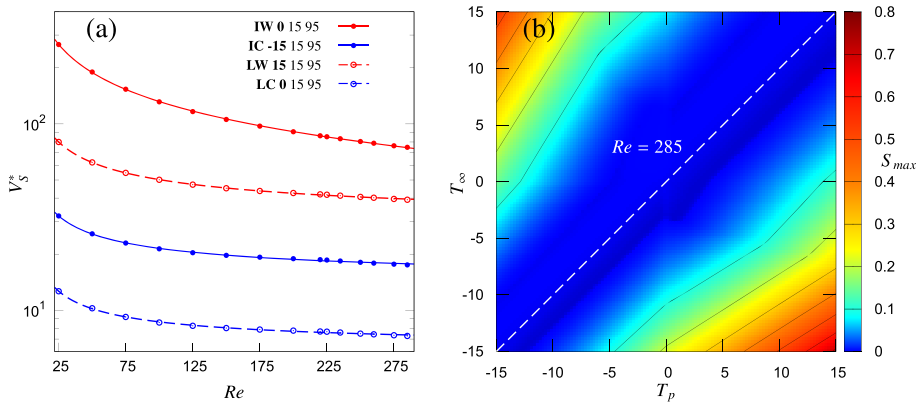

Figure 2. The evolution of supersaturation in the wake. (a) The supersaturated volume $V_S^* = V_S/(\pi d_p^3/6)$ is plotted against different Re, considering both (I) frozen and (L) liquid hydrometeors with both (W) warmer or (C) colder temperature than the ambient, while maintaining $\Delta T = 15°C$ and $RH_\infty = 95\%$. The dots are simulation results, while the lines correspond to the $C_0(1 + C_1 Re^\alpha)$ fitting model. Solid dots/lines represent frozen hydrometeors and the empty dots/dashed lines represent liquid hydrometeors, with red and blue color for warmer and colder hydrometeors respectively. (b) Supersaturation maximum S_{max} for different values of T_p and T_∞ varying from -15°C to 15°C for $Re = 285$ keeping $RH_\infty = 95\%$. Black contour lines are drawn for each 0.1 increase in S_{max}.

temperature than the ambient. The coefficient C_1 and the exponent α show a minor sensitivity to the thermodynamic parameters, as C_1 is between 10 and 13 and α is -0.63 ± 0.02 for our simulations. The data only deviates significantly when the supersaturated region is not completely within the computational domain (e.g., the case of warmer ice hydrometeors at higher Reynolds number and in almost saturated ambient), and we thus consider this a numerical artifact. We observed that the $Re^{-0.63}$ scaling of the supersaturated volume closely follows the scaling of the drag coefficient with the Reynolds number in the investigated range of Re (Clift et al., 1978). Thus, the decrease in V_S follows the dynamics of the wake, as also Figure 1a suggests. This aspect requires, however, further quantitative investigation.

Figure 2b shows the development of the maximum supersaturation S_{max} over a wide range of hydrometeor temperature T_p and ambient temperature T_∞ at a fixed Reynolds number $Re = 285$ and an ambient relative humidity $RH_\infty = 95\%$ for both (I) frozen and (L) liquid hydrometeors with both (W) warmer or (C) colder temperature than the ambient. The diagonal in white dashed line corresponds to $T_p = T_\infty$ and divides the plane into the colder hydrometeor case (top left) and the warmer hydrometeor case (bottom right). The temperature difference ΔT plays a crucial role, since S_{max} increases almost exponentially with it at a constant RH_∞. Similar to V_S, warmer hydrometeors generally produce a higher supersaturation maximum than colder hydrometeors at the same ΔT, regardless of their frozen or liquid state. The only exception happens in a nearly saturated ambient at $T_\infty = 0°C$, because the warmer hydrometeor is a liquid one while the colder one is frozen. In addition, S_{max} evolves almost independently of Re for various thermodynamic conditions. For details see section S7 in the supporting information.

3.2. Residence Time of Aerosols in the Wake

Atmospheric aerosols, which can be activated as a CCN or an INP, behave as passive tracers due to their very small inertia, so that their relaxation time is much smaller than the flow timescales and, therefore, their Stokes numbers are negligible. The present work does not consider inertial effects also on the motions of the activated aerosol particles and models them as passive tracers. To understand the possible role of the supersaturated hydrometeor wake on the aerosol activation, we have analyzed the trajectories of passive tracers injected upstream of the hydrometeor. Since only tracers starting their motion near the center line $y = z = 0$ can enter the supersaturated regions, two injection patterns are used: a coarse pattern where 2,601 tracers are injected uniformly over an area of $[1.5d_p \times 1.5d_p]$ and a fine pattern where 1,681 tracers are injected uniformly over an area of $[0.2d_p \times 0.2d_p]$ in the inlet around the hydrometeor center line. An adaptive Runge-Kutta 4–5 method is used for time integration of the trajectories. Velocity, temperature, and vapor density at the tracer position are obtained by trilinear interpolation.

The possibility of an aerosol being activated as a CCN depends both on the instantaneous supersaturation it experiences and on the time it spends in highly supersaturated regions (residence time), so that it reaches

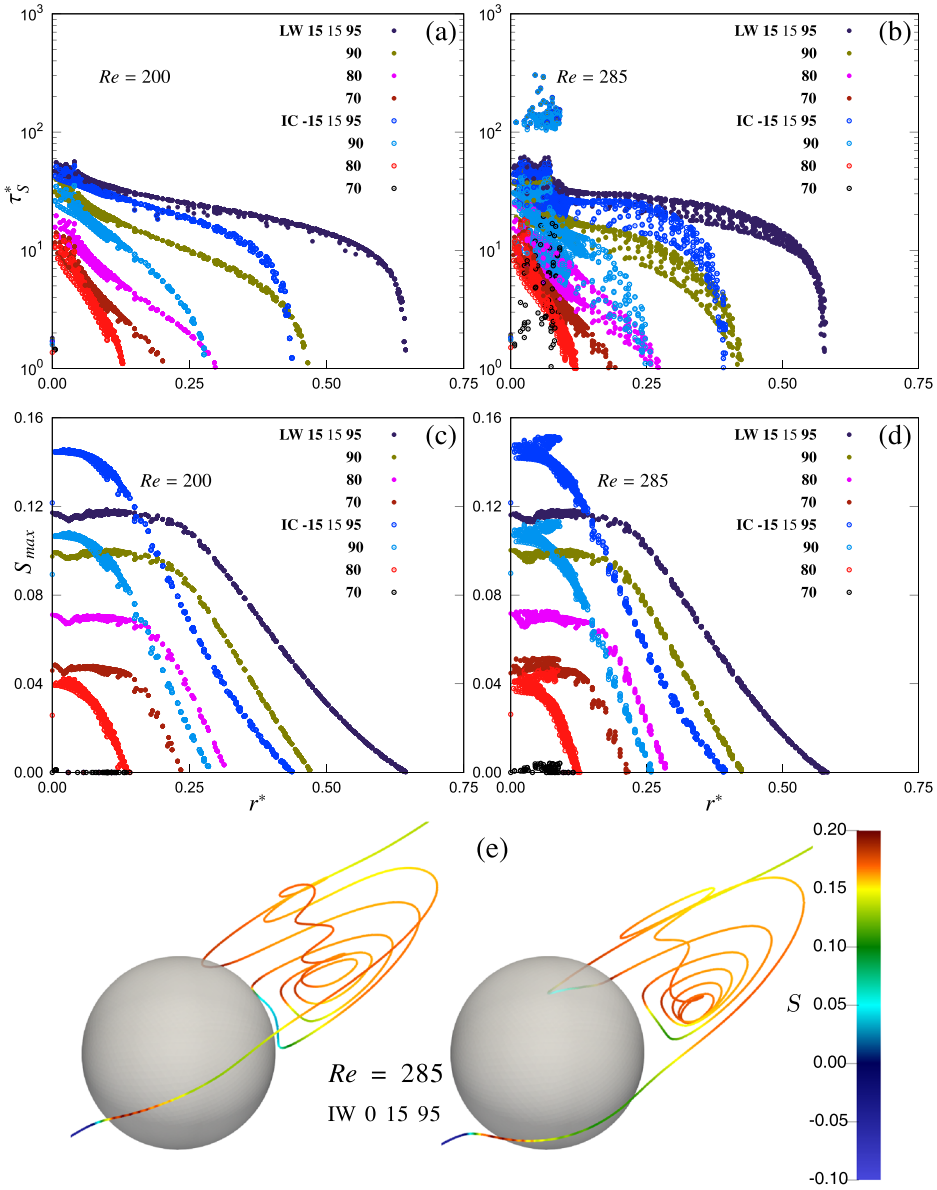

Figure 3. The residence time $\tau_S^* = \tau_S/(d_p/U_p)$ of a tracer within the supersaturated zone and the maximum supersaturation S_{max} experienced by a tracer are plotted as a function of the initial radial distance $r^* = r/d_p$ from the hydrometeor center line ($y = z = 0$). The evolution of τ_S^* within the $S > 1 \times 10^{-4}$ zone is plotted for $Re = 200$ in (a) and for $Re = 285$ in (b), while S_{max} is plotted for $Re = 200$ in (c) and for $Re = 285$ in (d). Various hydrometeor phases and RH_∞ conditions are considered keeping $\Delta T = 15°C$ and $T_\infty = 0°C$. Solid and empty dots represent the liquid warm and frozen cold hydrometeor conditions, respectively. In (e), two example tracer trajectories for $Re = 285$ are shown, colored according to the instantaneous S it experiences in an "IW 0 15 95" setup, resulting in $\tau_S^* = 151$ s (left) and $\tau_S^* = 145.4$ s (right).

a critical size that prevents its complete evaporation/sublimation according to the Köhler curve (Seinfeld & Pandis, 2006). The activation of an aerosol as an INP depends on many physical and chemical parameters, but, even for initiations of the INPs, a sufficient long residence time in a supersaturated region is required. Moreover, the activated CCNs can also grow to be INPs, through immersion freezing or contact freezing or homogeneous freezing of the liquid water (Hoose & Möhler, 2012). In Figure 3 we therefore plot the residence time τ_S that a tracer spends within the supersaturated wake in panels a and b, and S_{max} that it sees in panels c and d as a function of the initial radial distance r of the tracer from the hydrometeor center line for axisymmetric ($Re = 200$) and oblique ($Re = 285$) wakes, respectively. The different structure of the wake creates clearly visible differences in the supersaturation experienced by the tracers. The tracers, which stay

for the longer time in the supersaturated region of axisymmetric $Re = 200$ wake, are introduced near the center line as shown in Figure 3a, so that they move through the supersaturated boundary layer and along the border of the wake. However, no tracers could enter the closed recirculating region, resulting τ_S at most in the order of $10^1 d_p/U_p$ for $Re = 200$.

In the oblique wake regime of $Re = 285$, shown in Figure 3b, tracers injected far from the axis show no significant qualitative difference in τ_S, and they experience lower S_{max} in Figure 3d for a short time. However, "lucky tracers" injected near the center line can enter the near wake vortical region and therefore remain trapped in the supersaturated recirculating zone for a longer time before moving downstream. This increases τ_S by a factor between 2.5 to 9 with respect to the bulk of the tracers injected from the same radial distance in the symmetric or oblique wake regimes. We quantify the extent of the injection region of lucky tracers with $\tau_S \geq 10^2 d_p/U_p$, which is confined to a radial distance of $r/d_p \leq 0.09$. The "capture efficiency" E, which is defined as the ratio between the total frontal area A_F of the tracers with $\tau_S \geq 10^2 d_p/U_p$ and the frontal area of the hydrometeor $\pi d_p^2/4$, is about 5×10^{-3} for $Re = 285$, while it is almost zero in the steady axisymmetric regime. The scatter in Figure 3b for $Re = 285$, which produces petal-like patterns at low r/d_p, is due to the lack of axial symmetry in the oblique wake regime. The larger extent of the supersaturated region generated by a warmer hydrometeor (solid dots) compared to a colder hydrometeor (empty dots) for the same ΔT and RH_∞ is also visible in Figure 3. This is evident from the slower decay of τ_S and S_{max} with r/d_p for warmer hydrometeors.

The mechanism allowing long residence times in the case of an oblique wake can be inferred from Figure 3e, which shows two sample tracer trajectories with $r/d_p = 0.078$ and 0.066, respectively, each of which enter the vortical oblique wake region at $Re = 285$. The colors of the trajectories represent the instantaneous supersaturation that the tracers experience. Such lucky tracers, introduced very near the hydrometeor center line, experience a sudden maximum of supersaturation $S \sim 20\%$, for a short time as they move through the boundary layer on the front of the sphere. Then the supersaturation gradually decreases along the trajectory to about 10%. Later, when the tracer is entrained within the recirculating oblique wake zone, it experiences higher supersaturation again, but for a longer time due to the low velocity and complex three-dimensional flow structures of this region. However, such entrainment phenomenon is only observed when the wake loses its symmetry, that is, in the oblique wake regime from $Re = 225$ in our simulations.

4. Implications for the Nucleation in Clouds

The extent of the supersaturated volume, the maximum supersaturation, and the residence time of an aerosol in the supersaturated wake of precipitating hydrometeors provide important insights on aerosol activation in the atmosphere. For the aerosol entrainment in the wake, the precipitating hydrometeor has to generate an oblique wake, which occurs for a precipitating spherical raindrop when the diameter is at least 1 mm. Since raindrops exceeding a diameter of 2 to 3 mm are very rare and occur mostly in thunderstorms (Pruppacher & Klett, 2010), and also to satisfy the need for higher temperature difference, it is evident that wake-induced supersaturation can happen mainly in deep convective clouds with fully glaciated, mixed phased, and various liquid-phased hydrometeors due to a large temperature variation (Yuan et al., 2010). From the results of the previous section, the entrainment rate of "lucky aerosols," which enter per unit time into the frontal capture area A_F of a hydrometeor and thus experience a long residence time inside the supersaturated wake, is estimated as

$$N = N_a U_p A_F = N_a U_p E \pi d_p^2/4.$$

Here E is the capture efficacy, which is about 5×10^{-3} for $Re = 285$ and almost zero in the steady axisymmetric regime. N_a is the typical aerosol concentration, which varies from $\mathcal{O}(10^8)$ to $\mathcal{O}(10^9)$ m^{-3} within the continental clouds and from $\mathcal{O}(10^7)$ to $\mathcal{O}(10^8)$ m^{-3} within the remote marine clouds (Pruppacher & Klett, 2010). Therefore, $\mathcal{O}(10^0)$ s^{-1} $\leq N \leq$ $\mathcal{O}(10^1)$ s^{-1} aerosols in continental clouds and $\mathcal{O}(10^{-1})$ s^{-1} $\leq N \leq$ $\mathcal{O}(10^0)$ s^{-1} aerosols in remote marine clouds experience a higher residence time and higher supersaturation in the wake when a raindrop of at least 1 mm diameter settles at its terminal velocity ($Re \simeq 285$). Measurements of the number density of raindrops above 1 mm show a wide variability, which can be estimated to be in the range of $\mathcal{O}(10^1) - \mathcal{O}(10^2)$ drops per cubic meter (e.g., Adirosi et al., 2016; Waldvogel, 1974, and others). This leads to an entrainment rate of aerosols in the drop wakes between $\mathcal{O}(10^0)$ and $\mathcal{O}(10^3)$ m^{-3} s^{-1}. Since the capture efficiency E increases with the Reynolds number (we use the E of $Re = 285$), this could be considered a conservative estimate.

The critical supersaturation required for the activation of aerosols as a CCN is achieved by solving the Köhler equation for its chemical compositions and size (e.g., Lohmann, 2015; McFiggans et al., 2006; Seinfeld & Pandis, 2006, and others). Since the critical supersaturation needed for the heterogeneous nucleation of common atmospheric aerosols rarely exceed 1–2% in a uniform environment, we may estimate the aerosol growth (see section S8 in the supporting information) during its residence time within the supersaturated wake by considering the average supersaturation, which is much higher than 2% for a temperature difference of 15°C between the hydrometeor and the ambient. Such estimation shows that inside such a supersaturated wake, an aerosol can grow well above its critical radius by deposition of water vapor and therefore be activated as a CCN. During a convective precipitation process of typically 20 min, $\mathcal{O}(10^3) - \mathcal{O}(10^6)$ m^{-3} new aerosols can therefore be activated in the wake of the precipitating hydrometeors, which replenish the activated particle concentration in clouds that typically vary in $\mathcal{O}(10^8) - \mathcal{O}(10^9)$ m^{-3} (Hudson & Noble, 2013; Rosenfeld et al., 2016). The cloud ambient temperature considered in this study is between -15°C and 15°C, a range where the concentration of INPs is much smaller than the concentration of CCNs inside the clouds (Hoose & Möhler, 2012; Petters & Wright, 2015). Moreover, since we have shown that warmer hydrometeors produce a larger supersaturated volume than the colder hydrometeors, CCN activation will likely dominate over direct INP nucleation. However, considering the deduced entrainment rate of the aerosols in the wake of the hydrometeors, it is expected that also at lower cloud temperatures ($\leq$ 20°C where a significant concentration of INPs are detected by Murray et al., 2012), still a significant fraction of cloud aerosols may activate in the wake initially as CCNs (depending on the temperature, supersaturation, aerosol chemical composition, and other physical parameters), and then part of such activated CCNs may produce INPs through condensation or immersion freezing (Murray et al., 2012) or by contact freezing (Hoose & Möhler, 2012), which cannot be inferred from this study because we cannot distinguish between CCN and INP activation. On the other hand, some CCNs may grow into supercooled cloud droplets that are also detected at very low cloud temperatures (Hogan et al., 2004) at which homogeneous freezing is observed in the laboratory experiments. Therefore, from this study, the relative importance of aerosol activation as INPs cannot be estimated due to the vast parameter space influencing it. However, we have obtained a quantification on the rate of aerosol entrainment in the wake-induced supersaturation and its activation potential as CCNs. It should be noted that this rate of activation of aerosols, either as CCNs or both as CCNs and INPs altogether during the process of convective precipitation, is comparable with the experiments of Mossop (1976) on secondary ice production during the growth of a graupel by rime splintering, and the in-field measurements of ice particle production rate by Harris-Hobbs and Cooper (1987), and the in-cloud measurements of secondary ice particles by Heymsfield and Willis (2014), whereas an explicit rate of CCN production inside the clouds is not found that the results from this study can be compared to. For an explicit quantification of wake-induced nucleation, a detailed microphysical study is required taking into account the full details of the changing atmospheric conditions and the particle evolution while falling through the convective clouds. In addition, the effects of other influencing factors, such as cloud free stream turbulence (Bagchi & Kottam, 2008), strong convective motions like central updraft or entrainment induced mixing (e.g., Bhowmick & Iovieno, 2019; Grabowski & Wang, 2013; Nair et al., 2020, and others), or strong downdraft during precipitation (Wang et al., 2016) may further influence this nucleation and activation rate, which needs to be carefully investigated.

5. Summary and Concluding Remarks

In this letter a detailed analysis of the supersaturation field and aersol activation around a spherical hydrometeor, which settles at its terminal velocity, for different atmospheric conditions is presented. The NS equation for the flow velocity and the one-way coupled AD equations for temperature and density of water vapor are solved with the LBM. The supersaturated volume V_S in the wake of steady axisymmetric regime ($Re \leq 220$) and oblique regime ($225 \leq Re \leq 285$) shows a $Re^{-0.63}$ decrease for the same thermodynamic conditions with increase in Re, whereas V_S is very sensitive to the temperature difference ΔT between the hydrometeor and the ambient and its relative humidity condition RH_∞, so that V_S at constant ΔT increases as RH_∞ increases, which means that a small amount of vapor diffusion from a warmer hydrometeor or cooling by a colder hydrometeor can easily supersaturate an almost saturated wake volume. However, when RH_∞ is fixed, ΔT plays a crucial role in V_S, since without an adequate ΔT, a negligible supersaturated volume is generated. In addition, persistently warmer hydrometeors than the ambient produces larger V_S than the colder ones. The supersaturation maximum S_{max} behaves qualitatively similar to V_S.

Lagrangian tracking of aerosols as passive tracers shows how the complex flow pattern of the oblique wake allows some lucky aerosols to be entrained within the recirculating wake, resulting in a higher residence time within the highly supersaturated vortical zone. Importantly, we found that such a long residence time within the highly supersaturated wake not only exposes the aerosols to a higher level of supersaturation compared to its nucleation barrier but also provides enough time for the growth by deposition of water vapor to exceed its critical size and therefore to be activated as a CCN. The frontal area of these lucky tracers entering the vortical but highly supersaturated oblique wake has a capture efficiency of $\sim 5 \times 10^{-3}$ with respect to the hydrometeor frontal area at $Re = 285$. Our analysis shows that wake-induced nucleation of aerosols during a convective precipitation of 20 min can generate $\mathcal{O}(10^3) - \mathcal{O}(10^6)$ m^{-3} new activated particles which can contribute to the life cycle of clouds.

Data Availability Statement

Additional data supporting the conclusions can be found in the supporting information. Data used in this paper are available online (at https://doi.org/10.5281/zenodo.3956524).

Acknowledgments
This research was funded by the Marie-Skłodowska Curie Actions (MSCA) under the European Union's Horizon 2020 research and innovation programme (Grant Agreement No. 675675), and an extension to program COMPLETE by Department of Applied Science and Technology, Politecnico di Torino. Scientific activities are carried out in Max Planck Institute for Dynamics and Self-Organization (MPIDS), and computational resources from HPC@MPIDS are gratefully acknowledged. Scientific comments and suggestions from the reviewers are also gratefully acknowledged. First author wishes to acknowledge Giuliana Donini, Guido Saracco, Mario Trigiante, and Paolo Fino for support.

References

Adirosi, E., Volpi, E., Lombardo, F., & Baldini, L. (2016). Raindrop size distribution: Fitting performance of common theoretical models. *Advances in Water Resources*, *96*, 290–305. https://doi.org/10.1016/j.advwatres.2016.07.010

Bagchi, P., & Kottam, K. (2008). Effect of freestream isotropic turbulence on heat transfer from a sphere. *Physics of Fluids*, *20*(7), 73305. https://doi.org/10.1063/1.2963138

Baker, B. A. (1991). On the nucleation of ice in highly supersaturated regions of clouds. *Journal of the Atmospheric Sciences*, *48*(16), 1904–1907. https://doi.org/10.1175/1520-0469(1991)048<1905:OTNOII>2.0.CO;2

Baker, M. B. (1997). Cloud microphysics and climate. *Science*, *276*(5315), 1072–1078. https://doi.org/10.1126/science.276.5315.1072

Bhowmick, T., & Iovieno, M. (2019). Direct numerical simulation of a warm cloud top model interface: Impact of the transient mixing on different droplet population. *Fluids*, *4*(3), 144. https://doi.org/10.3390/fluids4030144

Bhowmick, T., Wang, Y., Iovieno, M., Bagheri, G., & Bodenschatz, E. (2020). Population distribution in the wake of a sphere. *Symmetry*, *12*(9), 1498. https://doi.org/10.3390/sym12091498

Bodenschatz, E., Malinowski, S. P., Shaw, R. A., & Stratmann, F. (2010). Can we understand clouds without turbulence? *Science*, *327*(5968), 970–971. https://doi.org/10.1126/science.1185138

Chouippe, A., Krayer, M., Uhlmann, M., Dušek, J., Kiselev, A., & Leisner, T. (2019). Heat and water vapor transfer in the wake of a falling ice sphere and its implication for secondary ice formation in clouds. *New Journal of Physics*, *21*(4), 43043. https://doi.org/10.1088/1367-2630/ab0a94

Clift, R., Grace, J., & Weber, M. (1978). *Bubbles, drops, and particles*: Academic Press.

Curtius, J. (2009). Nucleation of atmospheric particles. *The European Physical Journal Conferences*, *1*, 199–209. https://doi.org/10.1140/epjconf/e2009-00921-0

DeMott, P. J., Möhler, O., Cziczo, D. J., Hiranuma, N., Petters, M. D., Petters, S. S., et al. (2018). The Fifth International Workshop on Ice Nucleation Phase 2 (FIN-02): Laboratory intercomparison of ice nucleation measurements. *Atmospheric Measurement Techniques*, *11*(11), 6231–6257. https://doi.org/10.5194/amt-11-6231-2018

Dusek, U., Frank, G. P., Hildebrandt, L., Curtius, J., Schneider, J., Walter, S., et al. (2006). Size matters more than chemistry for cloud-nucleating ability of aerosol particles. *Science*, *312*(5778), 1375–1378. https://doi.org/10.1126/science.1125261

Dye, J. E., & Hobbs, P. V. (1968). The influence of environmental parameters on the freezing and fragmentation of suspended water drops. *Journal of the Atmospheric Sciences*, *25*(1), 82–96. https://doi.org/10.1175/1520-0469(1968)025<0082:TIOEPO>2.0.CO;2

Field, P. R., Lawson, R. P., Brown, P. R. A., Lloyd, G., Westbrook, C., Moisseev, D., et al. (2017). Secondary ice production: Current state of the science and recommendations for the future. *Meteorological Monographs*, *58*, 7.1–7.20. https://doi.org/10.1175/AMSMONOGRAPHS-D-16-0014.1

Fukuta, N., & Lee, H. J. (1986). A numerical study of the supersaturation field around growing graupel. *Journal of the Atmospheric Sciences*, *43*(17), 1833–1843. https://doi.org/10.1175/1520-0469(1986)043<1833:ANSOTS>2.0.CO;2

Gagin, A. (1972). The effect of supersaturation on the ice crystal production by natural aerosols. *Journal de Recherches Atmosphriques*, *6*, 175–185.

Grabowski, W. W., & Wang, L.-P. (2013). Growth of cloud droplets in a turbulent environment. *Annual Review of Fluid Mechanics*, *45*(1), 293–324. https://doi.org/10.1146/annurev-fluid-011212-140750

Guo, Z., Zheng, C., & Shi, B. (2002). An extrapolation method for boundary conditions in lattice Boltzmann method. *Physics of Fluids*, *14*(6), 2007–2010. https://doi.org/10.1063/1.1471914

Hader, J. D., Wright, T. P., & Petters, M. D. (2014). Contribution of pollen to atmospheric ice nuclei concentrations. *Atmospheric Chemistry and Physics*, *14*(11), 5433–5449. https://doi.org/10.5194/acp-14-5433-2014

Harris-Hobbs, R. L., & Cooper, W. A. (1987). Field evidence supporting quantitative predictions of secondary ice production rates. *Journal of the Atmospheric Sciences*, *44*(7), 1071–1082. https://doi.org/10.1175/1520-0469(1987)044<1071:FESQPO>2.0.CO;2

Heymsfield, A., & Willis, P. (2014). Cloud conditions favoring secondary ice particle production in tropical maritime convection. *Journal of the Atmospheric Sciences*, *71*(12), 4500–4526. https://doi.org/10.1175/JAS-D-14-0093.1

Hogan, R. J., Behera, M. D., O'Connor, E. J., & Illingworth, A. J. (2004). Estimate of the global distribution of stratiform supercooled liquid water clouds using the LITE lidar. *Geophysical Research Letters*, *31*, L05106. https://doi.org/10.1029/2003GL018977

Hoose, C., & Möhler, O. (2012). Heterogeneous ice nucleation on atmospheric aerosols: a review of results from laboratory experiments. *Atmospheric Chemistry and Physics*, *12*(20), 9817–9854. https://doi.org/10.5194/acp-12-9817-2012

Huang, J. (2018). A simple accurate formula for calculating saturation vapor pressure of water and ice. *Journal of Applied Meteorology and Climatology*, *57*(6), 1265–1272. https://doi.org/10.1175/JAMC-D-17-0334.1

Huang, Y., Blyth, A. M., Brown, P. R. A., Choularton, T. W., & Cui, Z. (2017). Factors controlling secondary ice production in cumulus clouds. *Quarterly Journal of the Royal Meteorological Society*, *143*(703), 1021–1031. https://doi.org/10.1002/qj.2987
Hudson, J. G., & Noble, S. (2013). CCN and vertical velocity influences on droplet concentrations and supersaturations in clean and polluted stratus clouds. *Journal of the Atmospheric Sciences*, *71*(1), 312–331. https://doi.org/10.1175/JAS-D-13-086.1
Huffman, P. J. (1973). Supersaturation spectra of agI and natural ice nuclei. *Journal of Applied Meteorology*, *12*(6), 1080–1082. https://doi.org/10.1175/1520-0450(1973)012<1080:SSOAAN>2.0.CO;2
Johnson, T. A., & Patel, V. C. (1999). Flow past a sphere up to a Reynolds number of 300. *Journal of Fluid Mechanics*, *378*, 19–70. https://doi.org/10.1017/S0022112098003206
Kanji, Z. A., Ladino, L. A., Wex, H., Boose, Y., Burkert-Kohn, M., Cziczo, D. J., & Krmer, M. (2017). Overview of ice nucleating particles. *Meteorological Monographs*, *58*, 1.1–1.33. https://doi.org/10.1175/AMSMONOGRAPHS-D-16-0006.1
Kotouč, M., Bouchet, G., & Dušek, J. (2009). Transition to turbulence in the wake of a fixed sphere in mixed convection. *Journal of Fluid Mechanics*, *625*, 205–248. https://doi.org/10.1017/S0022112008005557
Krayer, M., Chouippe, A., Uhlmann, M., Dušek, J., & Leisner, T. (2020). On the ice-nucleating potential of warm hydrometeors in mixed-phase clouds. *Atmospheric Chemistry and Physics Discussions*, *2020*, 1–21. https://doi.org/10.5194/acp-2020-136
Kreidenweis, S. M., Petters, M., & Lohmann, U. (2019). 100 years of progress in cloud physics, aerosols, and aerosol chemistry research. *Meteorological Monographs*, *59*, 11.1–11.72. https://doi.org/10.1175/AMSMONOGRAPHS-D-18-0024.1
Krüger, T., Kusumaatmaja, H., Kuzmin, A., Shardt, O., Silva, G., & Viggen, E. M. (2017). *Lattice Boltzmann method: Fundamentals and engineering applications with computer codes*: Springer, Cham. https://doi.org/10.1007/978-3-319-44649-3_8
Latt, J., Malaspinas, O., Kontaxakis, D., Parmigiani, A., Lagrava, D., Brogi, F., et al. (2020). Palabos: Parallel lattice boltzmann solver. *Computers & Mathematics with Applications*. https://doi.org/10.1016/j.camwa.2020.03.022
Lohmann, U. (2015). AEROSOLS | Aerosol-cloud interactions and their radiative forcing, (Second Edition). In G. R. North, J. Pyle, F. Zhang (Eds.), *Encyclopedia of Atmospheric Sciences (Second Edition)* (pp. 17–22). Oxford: Academic Press. https://doi.org/10.1016/B978-0-12-382225-3.00052-9
McFiggans, G., Artaxo, P., Baltensperger, U., Coe, H., Facchini, M. C., Feingold, G., et al. (2006). The effect of physical and chemical aerosol properties on warm cloud droplet activation. *Atmospheric Chemistry and Physics*, *6*(9), 2593–2649. https://doi.org/10.5194/acp-6-2593-2006
Meyers, M. P., DeMott, P. J., & Cotton, W. R. (1992). New primary ice-nucleation parameterizations in an explicit cloud model. *Journal of Applied Meteorology*, *31*(7), 708–721. https://doi.org/10.1175/1520-0450(1992)031<0708:NPINPI>2.0.CO;2
Michaelides, E. E. (2006). *Particles, bubbles and drops*: World Sceintific. https://doi.org/10.1142/6018
Montgomery, R. B. (1947). Viscosity and thermal conductivity of air and diffusivity of water vapor in air. *Journal of Meteorology*, *4*(6), 193–196. https://doi.org/10.1175/1520-0469(1947)004<0193:VATCOA>2.0.CO;2
Mossop, S. C. (1976). Production of secondary ice particles during the growth of graupel by riming. *Quarterly Journal of the Royal Meteorological Society*, *102*(431), 45–57. https://doi.org/10.1002/qj.49710243104
Murray, B. J., O'Sullivan, D., Atkinson, J. D., & Webb, M. E. (2012). Ice nucleation by particles immersed in supercooled cloud droplets. *Chemical Society Reviews*, *41*, 6519–6554.
Nair, V., Heus, T., & van Reeuwijk, M. (2020). Dynamics of subsiding shells in actively growing clouds with vertical updrafts. *Journal of the Atmospheric Sciences*, *77*(4), 1353–1369. https://doi.org/10.1175/JAS-D-19-0018.1
Petters, M. D., & Wright, T. P. (2015). Revisiting ice nucleation from precipitation samples. *Geophysical Research Letters*, *42*, 8758–8766. https://doi.org/10.1002/2015GL065733
Prabhakaran, P., Kinney, G., Cantrell, W., Shaw, R. A., & Bodenschatz, E. (2020). High supersaturation in the wake of falling hydrometeors: Implications for cloud invigoration and ice nucleation. *Geophysical Research Letters*, *47*, e2020GL088055. https://doi.org/10.1029/2020GL088055
Prabhakaran, P., Weiss, S., Krekhov, A., Pumir, A., & Bodenschatz, E. (2017). Can hail and rain nucleate cloud droplets? *Physical Review Letters*, *119*, 128,701. https://doi.org/10.1103/PhysRevLett.119.128701
Pruppacher, H. R., & Klett, J. D. (2010). *Microphysics of clouds and precipitation* (second). Dordrecht: Springer. https://doi.org/10.1007/978-0-306-48100-0
Qian, Y., D'Humières, D., & Lallemand, P. (1992). Lattice BGK models for Navier-Stokes equation. *Europhysics Letters*, *17*(6), 479–484.
Rosenfeld, D., Zheng, Y., Hashimshoni, E., Pöhlker, M. L., Jefferson, A., Pöhlker, C., et al. (2016). Satellite retrieval of cloud condensation nuclei concentrations by using clouds as CCN chambers. *Proceedings of the National Academy of Sciences*, *113*(21), 5828–5834. https://doi.org/10.1073/pnas.1514044113
Seinfeld, J. H., & Pandis, S. N. (2006). *Atmospheric chemistry and physics: From air pollution to climate change* (2nd ed.). New York: John Wiley & Sons.
Siebert, H., & Shaw, R. A. (2017). Supersaturation fluctuations during the early stage of cumulus formation. *Journal of the Atmospheric Sciences*, *74*(4), 975–988. https://doi.org/10.1175/JAS-D-16-0115.1
Silva, G., & Semiao, V. (2012). First- and second-order forcing expansions in a lattice Boltzmann method reproducing isothermal hydrodynamics in artificial compressibility form. *Journal of Fluid Mechanics*, *698*, 282–303. https://doi.org/10.1017/jfm.2012.83
Stevens, B., & Bony, S. (2013). What are climate models missing? *Science*, *340*(6136), 1053–1054. https://doi.org/10.1126/science.1237554
Succi, S. (2001). *Lattice Boltzmann equation for fluid dynamics and beyond*. Oxford: Clarendon Press.
Tian, F.-B., Wang, Y., Liu, H., & Zhang, Y. (2018). The lattice Boltzmann method and its applications in complex flows and fluid-structure interactions. *Proceedings of the Institution of Mechanical Engineers, Part C: Journal of Mechanical Engineering Science*, *232*(3), 403–404. https://doi.org/10.1177/0954406218754913
Tomboulides, A. G., & Orszag, S. A. (2000). Numerical investigation of transitional and weak turbulent flow past a sphere. *Journal of Fluid Mechanics*, *416*, 45–73. https://doi.org/10.1017/S0022112000008880
Waldvogel, A. (1974). The N_0 jump of raindrop spectra. *Journal of the Atmospheric Sciences*, *31*(4), 1067–1078. https://doi.org/10.1175/1520-0469(1974)031<1067:TJORS>2.0.CO;2
Wang, J., Krejci, R., Giangrande, S., Kuang, C., Barbosa, H. M. J., Brito, J., et al. (2016). Amazon boundary layer aerosol concentration sustained by vertical transport during rainfall. *Nature*, *539*(7629). https://doi.org/10.1038/nature19819
Yuan, T., Martins, J. V., Li, Z., & Remer, L. A. (2010). Estimating glaciation temperature of deep convective clouds with remote sensing data. *Geophysical Research Letters*, *37*, L08808. https://doi.org/10.1029/2010GL042753